J. Nucl. Phys. Mat. Sci. Rad. A. Vol. 8, No. 2 (2021), pp.177–182

CHITKARA

Journal of Nuclear Physics, Material Sciences, Radiation and Applications
Journal homepage: https://jnp.chitkara.edu.in/

Receptor Binding Domain (RBD) Structural Susceptibility in the SARS-CoV-2 Virus Spike Protein Exposed to a Pulsed Electric Field

V.J. Muñiz-Orozco[1], C.P. González[1], M. Fuentes-Acosta[1,3], J. Mulia-Rodríguez[1], L.A. Mandujano-Rosas[2,3] and D. Osorio-González[1,3*]

[1]*Molecular Biophysics Laboratory of the Faculty of Sciences, Autonomous University of the State of Mexico, Mexico*
[2]*Molecular Biophysics Modeling and Prototyping Laboratory, Mexiquense University, S. C., State of Mexico, Mexico*
[3]*Center for Research, Technology Transfer and Business Innovations. CITTIES, México*

[*]dog@uaemex.mx (Corresponding Author)

ARTICLE INFORMATION

Received: September 28, 2020
Accepted: January 27, 2021
Published Online: February 10, 2021

Keywords:
SARS-CoV-2, COVID-19, Receptor-Binding Domain (RBD)

DOI: 10.15415/jnp.2021.82023

ABSTRACT

SARS-CoV-2 is responsible for causing the Coronavirus disease 2019 (COVID-19) pandemic, which has so far infected more than thirty million people and caused almost a million deaths. For this reason, it has been a priority to stop the transmission of the outbreak through preventive measures, such as surface disinfection, and to establish bases for the design of an effective disinfection technique without chemical components. In this study, we performed *in silico* analysis to identify the conformational alterations of the SARS-CoV-2 *Spike* Receptor Binding Domain (RBD) caused by the effect of a pulsed electric field at two different intensities. We found that both stimuli, especially the one with the highest angular frequency and amplitude, modified the electrical charge distribution in the RBD surface and the number of hydrogen bonds. Moreover, the secondary structure was significantly affected, with a decrease of the structured regions, particularly the regions with residues involved in recognizing and interacting with the receptor ACE2. Since many regions suffered conformational changes, we calculated RMSF and ΔRMSF to identify the regions and residues with larger fluctuations and higher flexibility. We found that regions conformed by 353-372, 453-464, and 470-490 amino acid residues fluctuate the most, where the first is considered a therapeutic target, and the last has already been characterized for its flexibility. Our results indicate that a pulsed electric field can cause loss of stability in the *Spike*-RBD, and we were able to identify the vulnerable sites to be used as a starting point for the development of viral inhibition or inactivation mechanisms.

1. Introduction

SARS-CoV-2 is responsible for causing the coronavirus 2019 disease (COVID-19) reported for the first time on December 19th of 2019 in Wuhan, China. By January 30th of 2020 was declared an international emergency, and later, on March 11th, the World Health Organization (WHO) declared the highest level of alarm and characterized COVID-19 as a pandemic. The *Spike* glycoprotein is an essential surface protein of the coronavirus since it initiates the infection process by interacting with the host receptor, the angiotensin-converting enzyme 2 (ACE2) [1]. This protein has three identical chains, each consisting of two subunits involved in the host cell fusion process. The general structure of SARS-CoV-2 RBD is very similar to SARS-CoV-1 RBD, with a mean square deviation (RMSD) of 1.5 Å for 174 aligned Cα. The stability of *Spike*, and its affinity to ACE2 is higher in SARS-CoV-2 (by ~10-20 fold), which is partly due to structural differences in the RBD; in fact, it has been suggested that these factors could explain the increased pathogenicity and infectivity of SARS-CoV-2 [2]. However, the reasons for RBD structural changes are still unclear, which is why it is relevant to study its dynamics and find inhibition or inactivation mechanisms for SARS-CoV-2.

The virus has infected more than thirty million persons worldwide, causing almost a million deaths [3]. SARS-CoV-2 represents a remarkable health risk due to its easy propagation and is facing health systems against a difficult challenge. Therefore, the immediate urgency has focused on strict precautionary measures to stop virus transmission; however, the primary disinfectants used against SARS-CoV-2 are chemical substances [4-5], and they have a massive environmental impact. For these reasons, it is necessary to know the susceptibilities of SARS-CoV-2 that can lead to the development of new and effective disinfection methods. In the present work, an *in silico* analysis was performed to identify the conformational alterations in the receptor-binding domain (RBD) of the SARS-CoV-2

ISSN No.: 2321-8649(Print) ISSN No.: 2321-9289(Online); Registration No. : CHAENG/2013/51628

Spike protein induced by a pulsed electric field at different frequencies. Pulsed electric fields (PEF) constitute a physical method that uses electrical intensity ranges, which have been widely used to develop technologies focused on the preservation of food as a non-thermal medium capable of inactivating enzymes and pathogenic microorganisms in liquid foods [6]; they also have been proven effective for microbial inactivation in wastewater. These techniques save energy and prevent the use of harmful chemicals [7-8]. The pulsed electric field effect is focused on the weakest chemical bonds, such as hydrogen bonds, Van der Waals forces, and electrostatic forces, which usually provide protein stability [9]. Consequently, the primary protein structure remains intact, while the secondary and tertiary structures are affected in different levels, causing enzymatic inactivation, monomer unfolding, aggregation, or complete denaturation [10-12].

2. Methods

2.1. Molecular Model

We obtained the SARS-CoV-2 Spike RBD structure from the experimentally determined spatial configuration in the RCBS Protein Data Bank repository with ID 6VXX. The missing residues were added using Homology Modeling through the SWISS-MODEL workspace. We used the GROMACS 2020 suite with the CHARMM36 force field for molecular simulation. The RBD was solvated with 36,798 water molecules using the TIP3P model inside a simulation box with rhombic dodecahedron geometry, and periodic boundary conditions were incorporated. Na^+ and Cl^- ions were added at a concentration of 0.15 mol / L for achieving electric neutrality in the system. An NVT (particle number, volume, and temperature remain constant) statistical assembly was used while controlling the temperature with the Berendsen thermostat. For energetic interactions, Van der Waals and Coulomb cutoff radius was set at 18 Å and 14 Å respectively. We carried out the energy minimization process using the steepest descent method, and afterward, the simulation was performed in 3 stages: i) Relaxation of the system, ii) Equilibration and iii) Production. The system energy stability was achieved in 50 ns, and the production stage was carried out for 1000 ns.

2.2. Structural Properties

The root mean square fluctuation per amino acid residue was calculated by

$$RMSF(i) = \left[\frac{1}{T}\sum_{t_1=1}^{T}\left\|r_i(t_1) - r_i(t_2)\right\|^2\right]^{\frac{1}{2}} \qquad (1)$$

Where $r_i(t_1)$ is the initial position of the atom i at time t_1, while $r_i(t_2)$ is the position at a later time.

2.3. Electric Field Model

The hydrated RBD was stimulated with a time-dependent pulsed electric field with a maximum at t_0 and width σ given by

$$E(t) = E_0 \exp\left[-\frac{(t-t_0)^2}{2\sigma^2}\right]\cos\left[\omega(t-t_0)\right] \qquad (2)$$

Where E_0 is the initial amplitude of the pulse whose angular frequency is in terms of the wavelength λ and the speed of light c, and is calculated using $\omega = \frac{2\pi c}{\lambda}$. The temperature was fixed at $T = 310K$, and structural variations inducted by two different electric fields were observed for 1000 ns; the parameters used for each stimulus are shown in Table 1.

Table 1: Values of the electric field parameters used to stimulate the RBD.

	E_0 (Vnm^{-1})	ω (ps^{-1})	t_0(ps)	σ (ps)
Electric Stimulus 1	1.5	150	5	1
Electric Stimulus 2	2.9	300	5	1

Ionization effects do not occur since $\lambda > 150\ nm$ [13]; furthermore, at average temperature, the water and RBD domain molecules vibration are at the same order than kT. Additionally, we do not consider any quantum effects, but the method contemplates quantum corrections through autocorrelation forces functions [14].

3. Results and Discussion

Using cryogenic electron microscopy, Walls and coworkers determined the structure of the closed conformation of SARS-CoV-2 *Spike* trimer at 2.8 Å resolution [15]. This structure is found in the Protein Data Bank repository with the ID 6VXX. Figure 1 shows the protein and emphasizes the RBD domain. Like many other biomolecules, the *Spike* protein has very flexible regions or some structural instability, so the resolution of the experiment may not capture some amino acid residues position. In the referred experiment, the *Spike* missing residues are 445-446, 454-461, and 469-488 (Fig. 1b). We used this structure atomic spatial coordinates to extract the RBD domain (329-521 residues) and completed it using homology modeling (Figure 1a and 1b). The structure we obtained comprises Spike residues 333 to 527, and achieved an acceptable approximation compared to the experimental structure (Fig. 1b).

RBD was subjected to two different stimuli using a pulsed electric field with the parameters shown in Table 1. Theoretical reports have suggested that electric field intensities of at least 0.10 Vnm^{-1} can cause subtle movements of atoms within proteins and promote conformational changes [16]. Moreover, in previous work, we used 1.0 Vnm^{-1} to induce structural variations in other viral proteins [17]. Based on the previous statements, we initially disturbed RBD with stimulus 1, and after that, we used a second stimulus $E^0 = 2.9\ Vnm^{-1}$ with twice the intensity: $\omega = 300\ ps^{-1}$ (Table 1).

Once the RBD domain was hydrated and equilibrated inside the simulation box, the two electrical stimuli were applied. The electric field propagation was verified through all the simulation space (rhombic dodecahedron), the electric potential and the charge density were monitored throughout the simulation process. Because the charge distribution in RBD is intrinsically related to the protein-protein and protein-ligand interactions, we calculated these distributions before and after the electrical stimulation; results are shown in Figure 2. Both stimuli promote the formation of large, negatively charged patches in the region 333-383. The higher effect was achieved under stimulus 1, which is best appreciated in the protein lateral views in the third column of Figure 2. In contrast, stimulus 2 generated a positively charged patch at the region 453-466, which is observed in the last column of figure 2. On the other hand, the region 468-487 was conspicuously negatively charged when stimulus 2 was applied.

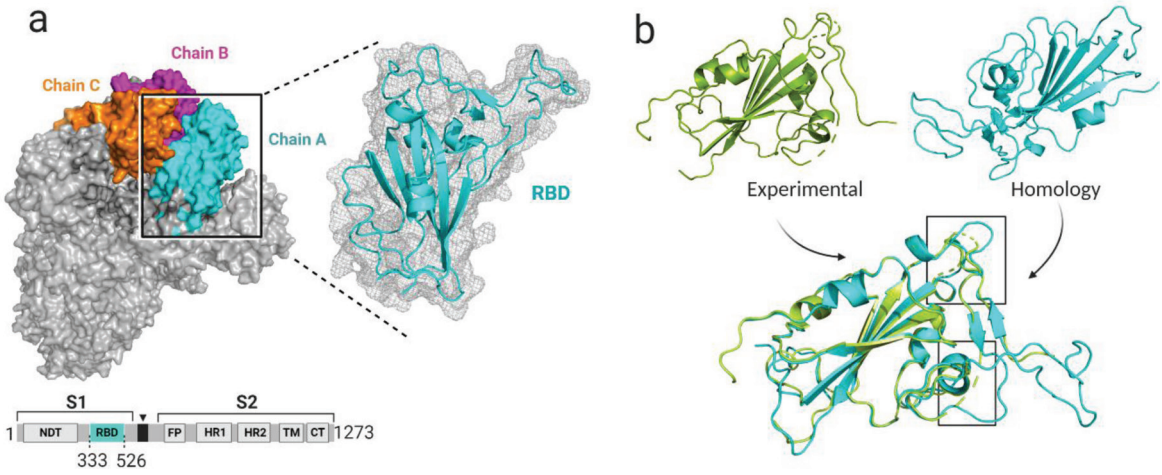

Figure 1: Structural organization of *Spike* and RBD. a) Left: *Spike* protein domain distribution, the arrow represents the cleavage site. Chain A (cyan), B (magenta), and C (orange) of RBD are emphasized. Right: The secondary structure of RBD constructed by homology modeling is shown. b) Experimental RBD structure (PDB ID 6VXX) and RBD obtained by homology modeling (residues 333-527). The alignment of both structures is shown below (RMSD= 0.682, 983 atoms), and the boxes highlight the missing regions in the experimental structure of RBD (445-446, 454-461 y 469-488).

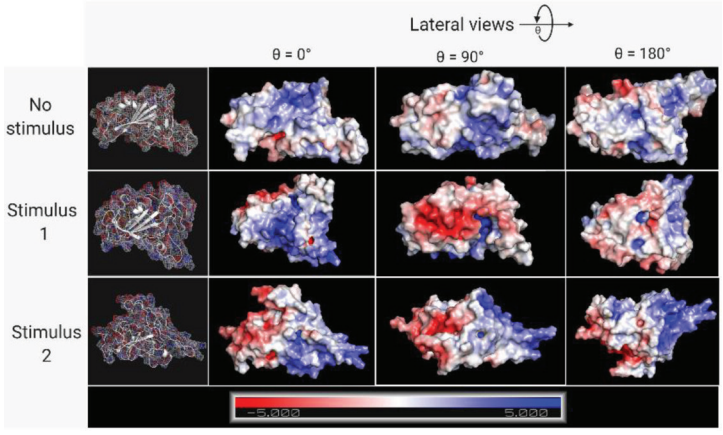

Figure 2: Electric charge distribution in RBD. Charge distribution comparison among the three protein states (no stimulus, stimulus 1, and stimulus 2). The RBD structures were aligned and oriented in the same direction; each column shows a lateral view of the RBD corresponding to horizontal rotations of 90°.

The electrical stimuli significantly affected the secondary structure of RBD. The number of hydrogen bonds decreased moderately under stimulus 1 and decreased drastically under stimulus 2, showing the loss of structural stability after applying a higher amplitude and frequency stimulus. The main changes observed after applying the stimulus 1 are the displacement and reduction of structured regions (Fig. 3a and 3b); particularly the residue K417, which was included in an α-helix (α), and the regions 404-410 (α), 452-454 (β) y 492-494 (β) changed to loops. After the stimulus 2 (Fig. 3c), 338-342 (α), 354-357 (β), 365-371 (α), 393-403 (α), 404-410 (α), 452-454 (β), and 492-494 (β) also switched to loops. Both stimuli affected the regions 452-454 and 492-494, which are involved in ACE2 recognition and contribute with 115 Van der Waals contacts in the interface with the receptor [18]; furthermore, Tyr453, Gln493, and Ser 494 are located in regions that contribute to the protein-receptor binding [18-20]; these β sheets together with 404-410 α-helix, are responsible for correctly positioning many residues to form a network of hydrogen bonds with ACE2 [18]. By changing the structure in these regions, the RBD might lose the ability to recognize and interact with the receptor, inhibiting the virion contagion mechanism.

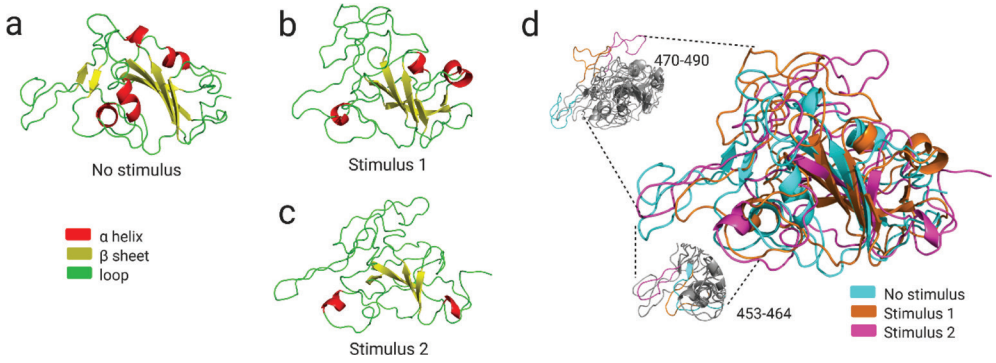

Figure 3: Secondary structure changes induced by electric stimuli. a) RBD without stimulus; b) RBD under stimulus 1; c) RBD under stimulus 2. d) Structural alignment; the highlighted regions show significant fluctuations.

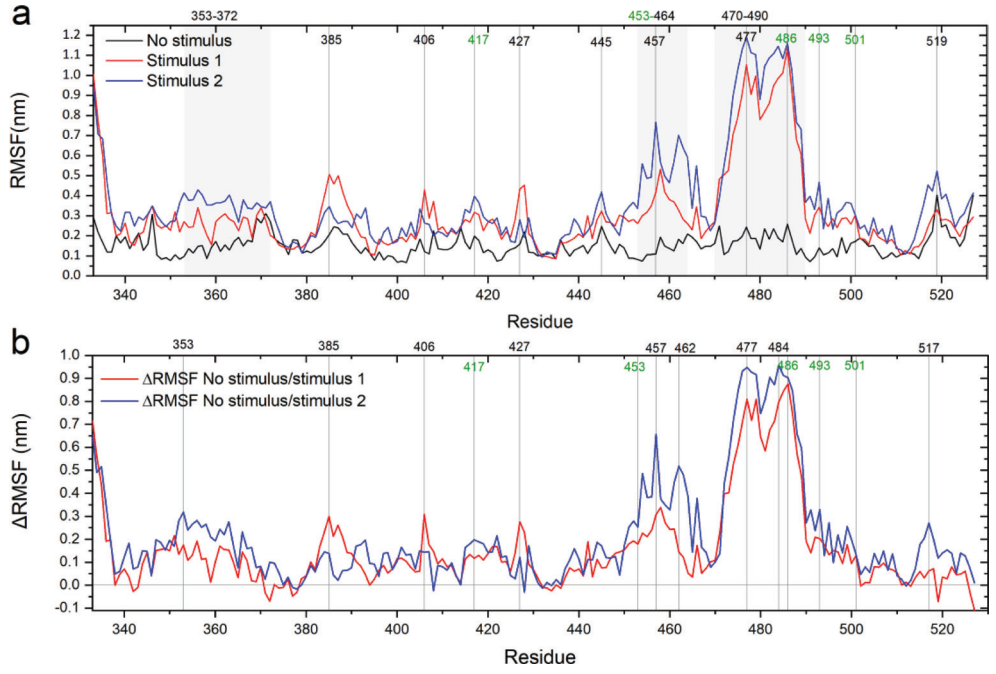

Figure 4: Comparison of the fluctuation between the three states to which the RBD was subjected. a) RMSF measures the average displacement of each residue in relation to the reference structure. The regions with the most noticeable changes are highlighted in gray. b) ΔRMSF represents the stimulated structure net displacement compared to the unstimulated structure. The amino acid residues identified in the literature as essential for RBD-ACE2 binding are shown in green.

The alignment of the three RBD structures allowed the visualization of important displacements or changes in the structure (Figure 3d). To support these observations, we calculated the RMSF (Figure 4a), a measure associated with structural flexibility. According to our analysis, the regions with significant fluctuations were 353-372, 453-464, and 470-490, which were especially affected under stimulus 2. The referred regions are located in non-structured zones (that tend to be more flexible), and the last two are part of the RBM. These results agree with previous reports where the region 470-490 was characterized as very flexible [2]. It is worth noting the fluctuations in K417, F486, and Y489 (3.0 Å, 9.1 Å y 6.1 Å, respectively); K417 is involved in the formation of salt bridges and hydrogen bonds with ACE2, while F486 and Y489 are included in hydrophobic interactions at the interface with the receptor [18].

We observe that even without an electrical stimulus, the RBD has fluctuations throughout the entire structure (Figure 5a); the RBD from SARS-CoV-2 has been qualified as a very flexible polypeptide, even more than the SARS-CoV-1 RBD [2]. Therefore, we calculated the ΔRMSF (Figure 4b), corroborating the previous results, and identified the residues with higher flexibility: Thr385, Glu406, Asp427, Ser477 and Phe486 under stimulus 1; Trp353, Tyr453, Arg457, Lys462, Ser477, Glu484, and Phe486 under stimulus 2. Interestingly, we found that the RBD residues that contribute to the *hinge* movement, 346-354 and 358-363 in our model, became more flexible under the stimuli, especially Trp353 and Ala363 (Figure 4a and 4b). Since it has been established that flexibility is critical in the receptor coupling dynamics of *Spike*, and therefore of RBD, alterations -such as those induced by stimuli- might have effects over viral-receptor interactions that might lead to viral inhibition or inactivation [21].

Conclusions

The *in silico* analysis showed that a pulsed electric field with $E_0 = 1.5\ Vnm^{-1}$, $\omega = 150\ ps^{-1}$, $t_0 = 5\ ps$, and $\sigma = 1\ ps$, modifies the structural conformation of some regions in RBD; in contrast, the stimulus with $E_0 = 2.9\ Vnm^{-1}$, $\omega = 300\ ps^{-1}$, $t_0 = 5\ ps$, and $\sigma = 1\ ps$, induces severe conformational changes. The pulsed electric field triggers the loss of protein stability; such structural instability is manifested mainly in a region including residues involved in the ACE2 recognition, which are also responsible for creating the hydrogen bonds network that allows the binding of the virion capsid with the cellular membrane initiating the fusion process. Likewise, our analysis allowed to identify the sites with higher susceptibility to conformational changes in the 353-372 region, whose structural dynamics in the presence of ACE2 is considerate the most efficient to achieve the molecular coupling in less time, and therefore is considered as a therapeutic target for the development of medical treatments against COVID-19. To our knowledge, there is no precedent of this region susceptibility to conformational changes in the coronavirus literature published so far. The flexibility exhibited by this region due to the pulsed electric field shows us a vulnerability of SARS-CoV-2, and constitutes one baseline to find practical, safe, and low-cost inactivation mechanisms.

Acknowledgements

The authors wish to express gratitude to the Center for Research, Technology Transfer, and Business Innovation (CITTIES) for supporting this project's development. Figures (1-3) were designed using BioRender.com.

References

[1] D. Wrapp, N. Wang, K.S. Corbett, J.A. Goldsmith, C.-L. Hsieh, O. Abiona, B.S. Graham and J.S. McLellan, Science **367**, 1260 (2020). https://doi.org/10.1126/science.abb2507

[2] J. He, H. Tao, Y. Yan, S.-U. Huang and Y. Xiao, Viruses **12**, 428 (2020). https://doi.org/10.3390/v12040428

[3] Worldometers.info. 2020. Retrieved from https://www.worldometers.info/coronavirus

[4] EPA de EE. UU. 2020. Retrieved from https://www.epa.gov/pesticide-registration/list-n-disinfectants-use-against-sars-cov-2

[5] Food and Drug Administration EE**.** UU. 2020. https://www.fda.gov/media/136289/download

[6] M.R. Robles-Lopez, R.R. Robles de la Torre, M. Camarillo-Cadena, A. Hernandez-Arana, J.S. Welti-Chanes and H. Hernandez-Sanchez, Revista Mexicana de Ingeniería Química (In English: Mexican Journal of Chemical Engineering) **11**, 373 (2012).

[7] J.P. Clark, Food Technology **60**, 60 (2006).

[8] W. Frey, C. Gusbeth, T. Sakugawa, M. Sack, G. Mueller, J. Sigler, E. Vorobiev, N. Lebovka, I. Álvarez, J. Raso, L.C. Heller, M.A. Malik, C. Eing and J. Teissie, Environmental Applications, Food and Biomass Processing by Pulsed Electric Fields, edited by H. Akiyama and R. Heller, *Bioelectrics*, (Springer, Tokyo, 2016) Chap. 6, pp. 389-476. https://doi.org/10.1007/978-4-431-56095-1_6

[9] H.W. Yeom, Q.H. Zhang and G.W. Chism, Journal of Food Science **67**, 2154 (2002). https://doi.org/10.1111/j.1365-2621.2002.tb09519.x

[10] L. Barsotti, E. Dumay, T.H. Mu, M.D.F. Diaz and J.C. Cheftel, Trends in Food Science & Technology **12**, 136 (2002). https://doi.org/10.1016/S0924-2244(01)00065-6

[11] O.E. Perez and A.M.R. Pilosof, Food Research International **37**, 102 (2004). https://doi.org/10.1016/j.foodres.2003.09.008

[12] R. Zhang, L. Cheng, L. Wang and Z. Guan, IEEE Transactions on Plasma Science **34**, 2630 (2006). https://doi.org/10.1109/TPS.2006.884800

[13] B. Winter and M. Faubel, Chemical Reviews **106**, 1176 (2006). https://doi.org/10.1021/cr040381p

[14] S.A. Egorov, K.F. Everitt and J.L Skiner, J. Phys. Chem A **103**, 9494 (1999). https://doi.org/10.1021/jp9919314

[15] A.C. Walls, Y.J. Park, M.A. Tortorici, A. Wall, A.T. McGuire and D. Veesler, Cell **181**, 281 (2020). https://doi.org/10.1016/j.cell.2020.02.058

[16] D.R. Hekstra, K.I. White, M.A. Socolich, R.W. Henning, V. Šrajer and R. Ranganathan, Nature **540**, 400 (2016). https://doi.org/10.1038/nature20571

[17] C. Peña-Negrete, M.A. Fuentes-Acosta, J. Mulia, L.A. Mandujano-Rosas and D. Osorio-González, Journal of Nuclear Physics, Material Sciences, Radiation and Applications **7**, 189 (2020). https://doi.org/10.15415/jnp.2020.72024

[18] Q. Wang, Y. Zhang, L. Wu, S. Niu, C. Song, Z. Zhang, G. Lu, C. Qiao, Y. Hu, K.-Y. Yuen, Q. Wang, H. Zhou, J. Yan and J. Qi, Cell **181**, 894 (2020). https://doi.org/10.1016/j.cell.2020.03.045

[19] Y. Wan, J. Shang, R. Graham, R.S. Baric and F. Li, Journal of virology **94**, 1 (2020). https://doi.org/10.1128/JVI.00127-20

[20] J. Lan, J. Ge, J. Yu, S. Shan, H. Zhou, S. Fan, Q. Zhang, X. Shi, Q. Wang, L. Zhang and X. Wang, Nature **581**, 7807 (2020). https://doi.org/10.1038/s41586-020-2180-5

[21] R. Melero et al., bioRxiv: the preprint server for biology 2020, (to be published). https://doi.org/10.1101/2020.07.08.191072

CHITKARA

Journal of Nuclear Physics, Material Sciences, Radiation and Applications

Chitkara University, Saraswati Kendra, SCO 160-161, Sector 9-C, Chandigarh, 160009, India

Volume 8, Issue 2 **February 2021** **ISSN 2321-8649**